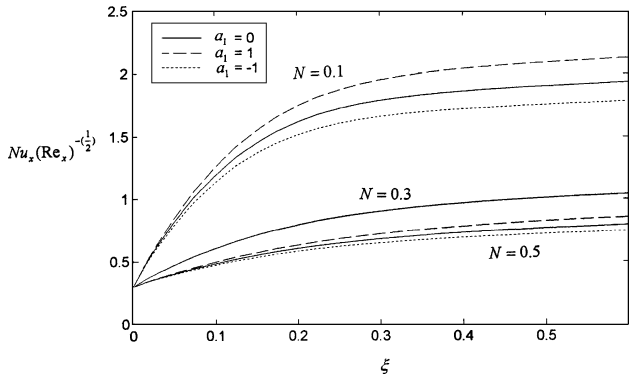

Fig. 3 Effects of the conduction-radiation parameter N on the value of the local Nusselt number for $Pr = 0.733$, $\omega = 0.5$, $\rho_d = 0$, $\Omega = 1$, and $\theta_w = 1.2$.

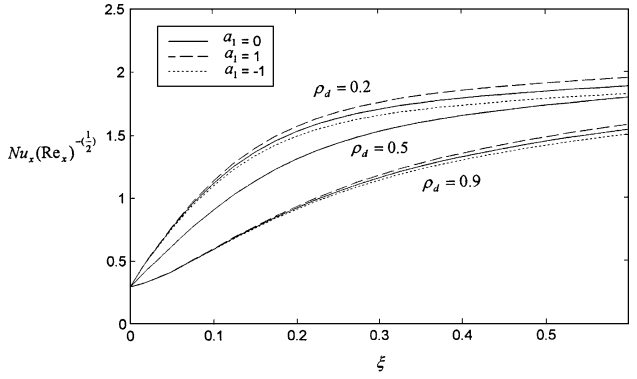

Fig. 4 Effects of the surface reflectivity ρ_d on the value of the local Nusselt number for $Pr = 0.733$, $\omega = 0.2$, $N = 0.1$, $\Omega = 1$, and $\theta_w = 1.2$.

is to decrease the value of the total heat flux at small values of ξ but to increase at large values of ξ, and the forward-backward-scattering parameter a_1 has a significant effect on the heat transfer. The value of the local Nusselt number for a strong backward-scattering fluid ($a_1 = -1$) with $\omega = 0.2$ is about 2.0% less than that for a strong forward-scattering fluid ($a_1 = 1$) at $\xi = 0.1$ and 3.5% less at $\xi = 0.6$, and the respective percentages are 21 and 38% for $\omega = 0.9$. The anisotropic scattering effects on the value of the local Nusselt number are amplified at large values of ω and the difference between the isotropic and Rayleigh scattering is small.

Figure 3 represents the variation of the local Nusselt number with the conduction-radiation parameter N, which characterizes the relative importance of radiation in regard to conduction. It is observed that the value of the local Nusselt number increases as the value of N decreases and the anisotropic scattering effects on the heat flux are amplified at small values of N.

Figure 4 shows the influence of the surface reflectivity. It is found that the value of the local Nusselt number decreases with the increase of surface reflectivity ρ_d. This is because the reflection at the surface increases the path length of radiative transfer.

Conclusions

From this study, the following is found:

1) The influence of the optical thickness τ_∞ is that the value of the net radiative heat flux and the local Nusselt number decreases as the optical thickness τ_∞ increases.

2) The effect of the scattering albedo ω is to decrease the value of the local Nusselt number at small values of ξ but to increase at large values of ξ.

3) The forward-backward-scattering parameter a_1 has a significant effect on the heat transfer.

4) The increase in the value of the local Nusselt number reduces the value of the conduction-radiation parameter N.

5) The value of local Nusselt number decreases with the increase of the value of surface reflectivity ρ_d.

6) The value of the local Nusselt number increases as the wall temperature increases.

References

[1]Cess, R. D., "The Interaction of Thermal Radiation with Free Convection Heat Transfer," *International Journal of Heat Mass Transfer*, Vol. 9, 1966, pp. 1269–1277.

[2]Arpaci, V. S., "Effect of Thermal Radiation on the Laminar Free Convection from a Heated Vertical Plate," *International Journal of Heat Mass Transfer*, Vol. 11, 1968, pp. 871–881.

[3]Soundalgekar, V. M., and Takhar, H. S., "Radiative Free Convection Flow of a Gas past a Semi-Infinite Vertical Plate," *Journal of Modern Measuring Contraction*, Vol. B51, 1993, pp. 31–40.

[4]Hossain, M. A., and Takhar, H. S., "Radiation Effect on Mixed Convection along a Vertical Plate with Uniform Surface Temperature," *International Journal of Heat and Mass Transfer*, Vol. 31, 1996, pp. 243–248.

[5]Cheng, E. H., and Özisik, M. N., "Radiation with Free Convection in an Absorbing, Emitting and Scattering Medium," *International Journal of Heat and Mass Transfer*, Vol. 15, 1972, pp. 1243–1252.

[6]Yücel, A., and Bayazitoglu, Y., "Radiative Heat Transfer in Absorbing, Emitting, and Anisotropically Scattering Boundary-Layer Flows," *AIAA Journal*, Vol. 22, No. 8, 1984, pp. 1162–1166.

[7]Wu, C. Y., Wu, S. C., and Chen, C. K., "Radiative Heat Transfer in Anisotropically Scattering Boundary-Layer Flows in Diffusely Reflecting Boundaries," *Proceedings of the Sixth International Numerical Methods in Thermal Problems Conference*, Vol. 6, Pt. 1, 1989, pp. 773–782.

[8]Chen, T. M., "Radiative Heat Transfer in Anisotropically Scattering Boundary-Layer Flows with Reflecting Boundaries," *International Journal of Heat and Mass Transfer*, Vol. 32, 1997, pp. 411–417.

[9]Cengel, Y. A., and Özisik, M. N., "The Use of the Galerkin Method for Radiation Transfer in an Anisotropically Scattering Slab with Reflecting Boundaries," *Journal of Quantum Spectroscopy Radiative Transfer*, Vol. 32, No. 3, 1984, pp. 225–233.

[10]Cebeci, T., and Bradshaw, P., *Momentum Transfer in Boundary Layers*, Hemisphere, Washington, DC, 1977.

Coupled Radiation and Conduction in a Graded Index Layer with Specular Surfaces

Yong Huang,* Xin-Lin Xia,† and He-Ping Tan‡
Harbin Institute of Technology, 150001 Harbin, People's Republic of China

Nomenclature

a_i	=	coefficient denoting temperature effect of node i on $I(x_k, \zeta_p)$
B_{ik}	=	coefficient denoting radiative effect of node i on thermal balance of node k
B'_{ik}	=	coefficient denoting temperature effect of node i on radiative flux of node k
d	=	thickness of medium layer, m
h	=	convective heat transfer coefficient, W/m$^2 \cdot$K
$I^*(j)$	=	radiative intensity at the jth tracing point, W/m$^2 \cdot$sr

Received 27 August 2002; revision received 7 October 2003; accepted for publication 2 November 2003.

*Ph.D. Candidate, School of Energy Science and Engineering, 92 West Dazhi Street; huangly_zl@263.net.

†Professor, School of Energy Science and Engineering, 92 West Dazhi Street; xiaxl@hit.edu.cn.

‡Professor, School of Energy Science and Engineering, 92 West Dazhi Street.

$I(x,\zeta)$	=	radiative intensity in medium, W/m$^2\cdot$sr
L	=	number of discrete solid angles
M	=	number of sublayers
N	=	conductive–radiative parameter, $\lambda\cdot\kappa/(4\sigma\cdot n_R^2\cdot T_R^3)$
$n(x)$	=	refractive index distribution
n_R	=	reference refractive index, 1.5
q^*	=	dimensionless heat flux, $q/\sigma\cdot T_R^4$
$S_{-\infty}, S_{+\infty}$	=	black surfaces denoting radiative surroundings
$s(j)$	=	curve length of the trajectory between the $(j-1)$th and the jth tracing points, m
T	=	temperature, K
T_R	=	reference temperature, $(T_{+\infty}+T_{-\infty})/2$, K
x	=	coordinate, m
Δx	=	sublayer thickness, m
ζ	=	polar angle of radiative propagation direction, rad
κ	=	absorption coefficient, m^{-1}
λ	=	thermal conductivity, W/m$\cdot$K
σ	=	Stefan–Boltzmann constant, 5.67×10^{-8} W/m$^2\cdot$K^4
τ	=	optical thickness, $\kappa\cdot d$
Θ	=	dimensionless temperature, T/T_R

Subscripts

c	=	conduction
$g1, g2$	=	gas flow outside surface
p	=	discrete direction of radiative propagation
r	=	radiation
t	=	coupled radiation and conduction
$-\infty, +\infty$	=	radiative surroundings $S_{-\infty}$ and $S_{+\infty}$, respectively

Introduction

FOR a semitransparent composite layer whose refractive index varies across an interface or surface but keeps constant within a layer, the coupled thermal radiation and heat transfer has been investigated by many researchers.[1–4] However, the thermal radiation in a graded index medium whose refractive index varies continuously has received little attention until recently. The pioneer work was contributed by Ben Abdallah and Le Dez, who put forward a curved ray tracing method to analyze the radiative transfer in graded index medium.[5,6] Following that, Lemonnier and Le Dez tried the discrete ordinate method,[7] and Huang et al.[8] and Xia et al.[9] combined the curved ray tracing method with a pseudo source-adding method to solve the problems with gray walls. Linear and sinusoidal refractive index distributions were considered in that research. In this paper, a numerical curved ray tracing (NCRT) method, recently developed by Huang et al.[10] is employed to investigate coupled radiation and conduction in a graded index semitransparent layer.

Analysis

The steady-state heat transfer of coupled radiation and conduction in a semitransparent medium layer is considered, as shown in Fig. 1. The absorption coefficient κ and thermal conductivity λ are kept constant in the medium, whereas the refractive index denoted by $n(x)$ is spatially variable. The two parallel plane boundaries are semitransparent specular surfaces, which reflect and refract thermal radiation by Fresnel's equation and Snell's law, respectively. In addition to the radiative surroundings denoted by two black walls $S_{-\infty}$ and $S_{+\infty}$, the convective effects of two transparent gas flows characterized by T_{g1}, h_1 and T_{g2}, h_2 respectively, are also considered in the boundary conditions. The thermal balance equation of heat transfer in the medium is[6]

$$\lambda\frac{\mathrm{d}^2T(x)}{\mathrm{d}x^2}+\kappa\left[2\pi\int_0^{\pi}I(x,\zeta)\sin\zeta\,\mathrm{d}\zeta-4n^2(x)\sigma T^4(x)\right]=0 \quad (1)$$

where $T(x)$, $I(x,\zeta)$, $n(x)$ are the temperature, the radiative intensity, and the refractive index, respectively. The radiative boundary conditions can be directly introduced during solving $I(x,\zeta)$, as will be shown in Eq. (5). The convective boundary conditions can be expressed as

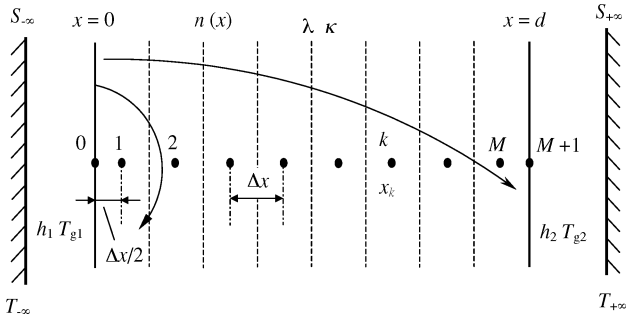

Fig. 1 Physical model and discretization.

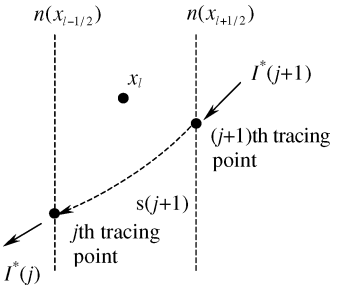

Fig. 2 Schematic of a curved ray tracing.

$$\lambda\frac{\mathrm{d}T(x)}{\mathrm{d}x}\bigg|_{x=0}=h_1\cdot[T(x)|_{x=0}-T_{g1}] \quad (2a)$$

$$\lambda\frac{\mathrm{d}T(x)}{\mathrm{d}x}\bigg|_{x=d}=h_2\cdot[T_{g2}-T(x)|_{x=d}] \quad (2b)$$

The thermal balance equation is numerically solved under the preceding boundary conditions. First, the medium is divided into M sublayers of equal thickness Δx, any of which is denoted by node k, and the two surfaces are represented by node 0 and node $M+1$, respectively. Then, the conductive term in Eq. (1) is discretized as that in Ref. 10, and the radiative term is solved by the NCRT method.[10]

Solution of Radiative Transfer

The essence of the NCRT method is to take advantage of the analytical solution of curved ray tracing for radiative transfer in a medium layer with linear refractive index.[5,6] In a sublayer k, the refractive index distribution $n(x)$ is replaced by a linear approximation, which is

$$n(x)=n\left(x_{k-\frac{1}{2}}\right)+\frac{x-x_{k-\frac{1}{2}}}{\Delta x}\left[n\left(x_{k+\frac{1}{2}}\right)-n\left(x_{k-\frac{1}{2}}\right)\right] \quad (3)$$

Under a linear distribution of refractive index, the curved trajectory of thermal radiation can be described by a set of recursion expressions that were first deduced by Ben Abdallah and Le Dez[5,6] and later improved by Huang et al.,[8] Xia et al.,[9] and Huang et al.[10] For any curved trajectory in a sublayer, a recursion expression can be obtained to solve for the radiative intensity, which has been deduced and presented in Ref. 10. For the case illustrated in Fig. 2, the corresponding recursion formula is

$$\frac{I^*(j)}{n^2\left(x_{l-\frac{1}{2}}\right)}=e^{-\kappa s(j+1)}\frac{I^*(j+1)}{n^2\left(x_{l+\frac{1}{2}}\right)}+\frac{\sigma T_l^4}{\pi}\left(1-e^{-\kappa s(j+1)}\right) \quad (4)$$

When striking a boundary surface, the radiative energy will be partly reflected and partly refracted out of the medium layer, or be totally reflected. The curved ray tracing process in the refractive direction will be terminated, whereas that in the reflective direction

is continued until the optical thickness of the curved trajectory is large enough to decrease the intensity of ray to be neglectable. The reflectivity is determined by Fresnel's equation, and the critical angle for total reflection is given by Snell's law.

When the earlier described ray tracing is used and the recursion expressions are resorted to, the radiative intensity of any node can be determined, which is related to the temperatures of the nodes along the propagation trajectory. The solution can be expressed as[10]

$$I(x_k, \zeta_p) = \frac{\sigma n^2(x_k)}{\pi}\left(\sum_{i=1}^{M} a_i T_i^4 + a_0 T_{-\infty}^4 + a_{M+1} T_{+\infty}^4\right) \quad (5)$$

For a nonlinear refractive index distribution, the coefficients a_i, a_0, and a_{M+1} are numerically determined by tracing the propagation trajectory.[10]

Resorting to Eq. (4), the discrete form of the integral item in Eq. (1) can be given and written as

$$\int_0^{\pi} I(x_k, \zeta) \sin\zeta \, \mathrm{d}\zeta = \sum_{p=1}^{L} I(x_k, \zeta_p) \sin\zeta_p \frac{\pi}{L}$$

$$= \frac{\sigma n^2(x_k)}{\pi}\left(\sum_{i=1}^{M} B_{ik} T_i^4 + B_{0,k} T_{-\infty}^4 + B_{M+1,k} T_{+\infty}^4\right) \quad (6)$$

Similar to the coefficients in Eq. (5), numerical results can be obtained for the coefficients B_{ik}, $B_{0,k}$, and $B_{M+1,k}$ (Ref. 10).

When Eq. (6) is combined with the discrete conductive term,[10] Eq. (1) is finally discretized into a set of algebraic expressions, and the convective boundary conditions can also be discretized easily. Then the temperature field of coupled radiation and conduction in the medium can be evaluated by an iterative algorithm. From the temperature field, the radiative flux in the medium can be calculated by the following equation[10]:

$$q_r(x_k) = 2\pi \int_0^{\pi} I(x_k, \zeta) \sin\zeta \cos\zeta \, \mathrm{d}\zeta$$

$$= 2\sigma n^2(x_k)\left(\sum_{i=1}^{M} B'_{ik} T_i^4 + B'_{0,k} T_{-\infty}^4 + B'_{M+1,k} T_{+\infty}^4\right) \quad (7)$$

where the coefficients are numerically determined as in Eq. (5).

Verification

The reliability of the NCRT method and the resulting accuracy as a function of the number of discrete sublayers and discrete solid angles have been discussed in detailed in Ref. 10. In the calculations for this paper, according to that investigation, the number of discrete sublayers is taken to be $M = 100$ and the number of discrete solid angles is $L = 300$. The minimum optical thickness of the trajectory for terminating a curved ray tracing process is 20.0, and the maximum error for iteration is 10^{-6}.

Results and Discussion

In the calculations, $T_{-\infty} = T_{g1} = 1000$ K, $T_{+\infty} = T_{g2} = 1500$ K, $h_1 = h_2 = \infty$, and these parameters are kept constant. Five refractive index distributions are investigated, which include two linear distributions, two sinusoidal distributions, and a constant one. The temperature distributions and the heat flux distributions are shown in Figs. 3 and 4, respectively. The straight lines in Fig. 4 represent the total heat flux q_t, and other curves represent the radiative heat flux q_r.

As shown in Fig. 3, the difference among the temperature fields under five refractive index distributions varies with the optical thickness τ and conductive–radiative parameter N. In the case of $\tau = 0.1$ and $N = 0.01$, the difference is very small, and the temperature curves are close to straight lines (Fig. 3a). That means, in this case, the medium absorption at any node is close to the thermal emission at the node temperature caused by pure heat conduction. As the optical thickness τ increases to 1.0, however, more radiative

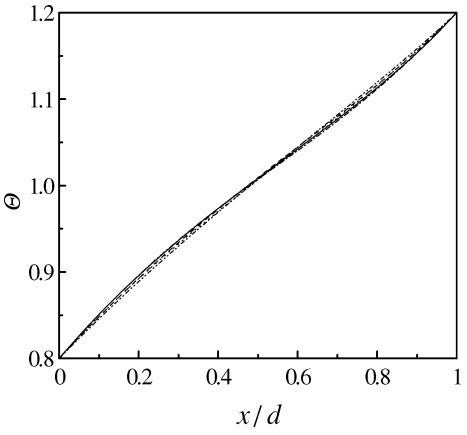

a) $\tau = 0.1$ and $N = 0.01$

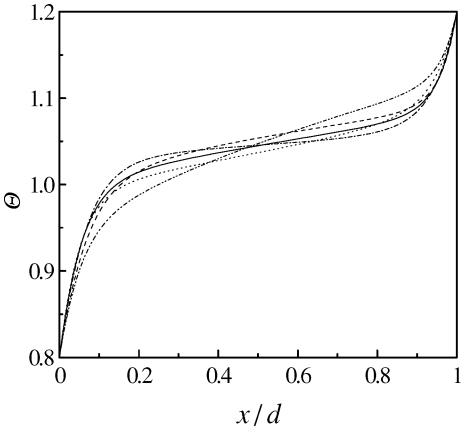

b) $\tau = 1.0$ and $N = 0.01$

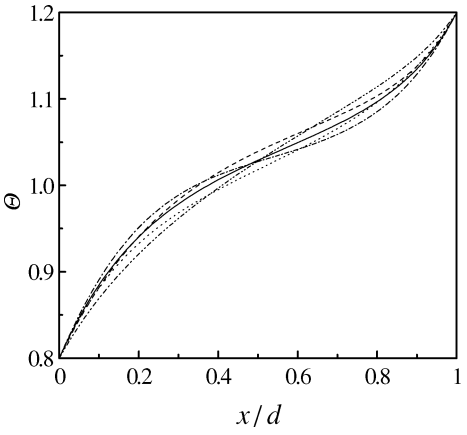

c) $\tau = 1.0$ and $N = 0.1$

Fig. 3 Dimensionless temperature field in the medium layer: ——, $n(x) = 1.5$; - - - -, $n(x) = 1.2 + 0.6x/d$; · · · ·, $n(x) = 1.8 - 0.6x/d$; - · - ·, $n(x) = 1.2 + 0.6\sin(\pi x/d)$; and - · · -, $n(x) = 1.8 - 0.6\sin(\pi x/d)$.

energy is absorbed by the medium, resulting in a rise of the average temperature (Fig. 3b). The radiative energy absorbed by a node near the low-temperature boundary increases to be more than the thermal emission at the node temperature caused by pure heat conduction, and so the temperature there increases. The situation is opposite for a node near the high-temperature boundary. Thus, the temperature curves become flat in the middle region. When the conductive–radiative parameter increases (Fig. 3c), the heat conduction in the regions near the two boundaries is enhanced. That weakens the temperature gradients near the boundaries, and slopes of the temperature curves increase again in the middle region.

Whether obvious or not, the influence of a refractive index distribution on temperature is similar for the three preceding cases.

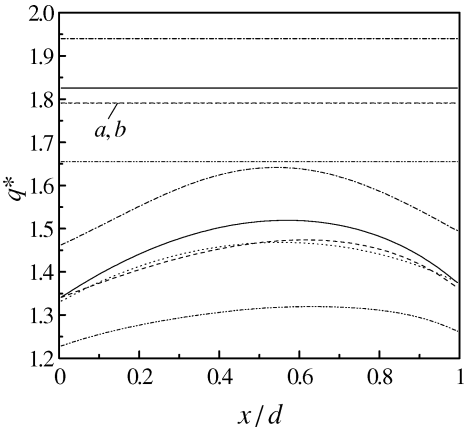

a) $\tau = 0.1$ and $N = 0.01$

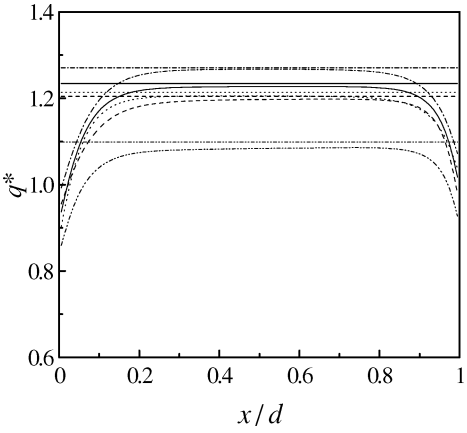

b) $\tau = 1.0$ and $N = 0.01$

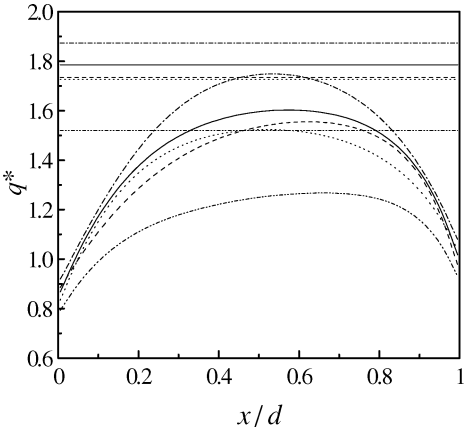

c) $\tau = 1.0$ and $N = 0.1$

Fig. 4 Dimensionless heat flux distribution in the medium layer: ——, $n(x) = 1.5$; - - - -, $n(x) = 1.2 + 0.6x/d$; · · · ·, $n(x) = 1.8 - 0.6x/d$; - · - ·, $n(x) = 1.2 + 0.6\sin(\pi x/d)$; and - · · -, $n(x) = 1.8 - 0.6\sin(\pi x/d)$.

Let us take the temperature distribution under a constant refractive index as a reference (solid lines), which is the average value due to a linear refractive index or a sinusoidal one. A refractive index distribution linearly increasing from the low-temperature surface to the high-temperature surface always leads to a higher temperature (dashed lines), and a decreasing linear refractive index distribution always causes a lower temperature (dotted lines). The sinusoidal refractive index with its peak value at the center of the medium, however, causes the temperature of the low-temperature region to be higher and that of the high-temperature region to be lower (dash–dot lines). Finally, the sinusoidal refractive index with its peak values at the boundaries causes the temperature of low-temperature region to be lower and that of the high-temperature region to be higher (dash–dot–dot lines). These differences among the temperature distributions are produced by total reflection in the medium.

The radiative heat flux is composed of two parts, one of which is from the surrounding radiation and the other is the medium emission. The former monotonically increases from the low-temperature surface to the high-temperature surface, but the latter varies in a complicated way. Thus, the radiative heat flux distributions in Fig. 4 are not monotonic. In the middle region of the medium, the radiative heat flux q_r is far larger than the conductive heat flux q_c ($q_c = q_t - q_r$), but in regions near the boundary, q_c can be larger than q_r (Fig. 4c). The total heat flux q_t drops as the optical thickness increases and rises with an increase in the conductive–radiative parameter. The radiative heat flux and total heat flux are significantly influenced by the refractive index distribution. A sinusoidal refractive index with its peak value at the medium center always leads to a greater heat flux than that for the reference refractive index (dash–dot lines), whereas a smaller heat flux is always caused by a sinusoidal refractive index with its peak value at the boundaries (dash–dot–dot lines).

Conclusions

From the investigation described, some elementary conclusions can be drawn. First, the NCRT method can be used to solve the radiative transfer in a graded index medium with semitransparent specular surfaces. Its flexibility in handling refractive index distribution and the resulting accuracy have been demonstrated. Second, at a temperature level above 1000 K, with an optical thickness greater than 0.1 and a conductive–radiative parameter less than 0.1, the influence of refractive index distribution on coupled radiation and conduction heat transfer is significant. Compared with the corresponding case under a constant refractive index, a linear refractive index always results in a higher temperature or a lower temperature. A sinusoidal refractive index always results in a higher heat flux or a lower one.

Acknowledgments

The project has been supported by the Fok Ying Tung Education Foundation (Grant 81050) and the National Natural Science Foundation of China (Grant 50336010). The authors are indebted to them for financial support.

References

[1]Siegel, R., and Spuckler, C. M., "Variable Refractive Index Effects on Radiation in Semitransparent Scattering Multilayered Regions," *Journal of Thermophysics and Heat Transfer*, Vol. 7, No. 4, 1993, pp. 624–630.

[2]Liou, B. T., and Wu, C. Y., "Radiative Transfer in a Multi-Layer Medium with Fresnel Interfaces," *International Journal of Heat and Mass Transfer*, Vol. 32, No. 1, 1996, pp. 103–107.

[3]Luo, J. F., Xia, X. L., and Tan, H. P., "Transient Coupled Heat Transfer in Three-Layer Composite with Opaque Specular Surfaces," *Journal of Thermophysics and Heat Transfer*, Vol. 16, No. 3, 2002, pp. 297–305.

[4]Tan, H. P., Luo, J. F., and Xia, X. L., "Transient Coupled Radiation and Conduction in a Three-Layer Composite with Semitransparent Specular Interfaces and Surfaces," *Journal of Heat Transfer*, Vol. 124, No. 3, 2002, pp. 470–481.

[5]Ben Abdallah, P., and Le Dez, V., "Temperature Field inside an Absorbing–Emitting Semitransparent Slab at Radiative Equilibrium with Variable Spatial Refractive Index," *Journal of Quantitative Spectroscopy and Radiative Transfer*, Vol. 65, No. 4, 2000, pp. 595–608.

[6]Ben Abdallah, P., and Le Dez, V., "Radiative Flux Field inside an Absorbing–Emitting Semitransparent Slab with Variable Spatial Refractive Index at Radiative Conductive Coupling," *Journal of Quantitative Spectroscopy and Radiative Transfer*, Vol. 67, No. 2, 2000, pp. 125–137.

[7]Lemonnier, D., and Le Dez, V., "Discrete Ordinates Solution of Radiative Transfer across a Slab with Variable Refractive Index," *Journal of Quantitative Spectroscopy and Radiative Transfer*, Vol. 73, No. 2, 2002, pp. 195–204.

[8]Huang, Y., Xia, X. L., and Tan, H. P., "Temperature Fields inside an Absorbing–Emitting Semi-Transparent Slab at Radiative Equilibrium with Linear Graded Index and Gray Walls," *Journal of Quantitative Spectroscopy and Radiative Transfer*, Vol. 74, No. 2, 2002, pp. 249–261.

[9]Xia, X. L., Huang, Y., and Tan, H. P., "Simultaneous Radiation and Conduction Heat Transfer in a Graded Index Semitransparent Slab with Gray Boundaries," *International Journal of Heat and Mass Transfer*, Vol. 45, No. 13, 2002, pp. 2673–2688.

[10]Huang, Y., Xia, X. L., and Tan, H. P., "Comparison of Two Methods for Solving Radiative Heat Transfer in a Graded Index Semitransparent Slab," *Numerical Heat Transfer, Part B*, Vol. 44, No. 1, 2003, pp. 83–99.

Two-Dimensional Hyperbolic Heat Conduction with Temperature-Dependent Properties

W. Shen* and S. Han†
Tennessee Technological University, Cookeville, Tennessee 38505

Nomenclature

c_p	=	specific heat at constant pressure
k	=	thermal conductivity
P	=	period of on–off heat flux
$q_{x(y)}$	=	$x(y)$ direction heat flux
T	=	temperature
Tr	=	reference temperature
t	=	time
α	=	thermal diffusivity ($k/\rho C_p$)
κ	=	fraction of period P
ρ	=	density
τ	=	relaxation time (α/c^2)

Introduction

THE phenomena of non-Fourier heat conduction are observed in many industrial applications, such as laser heating, cryogenic engineering, and nanotechnology. Various conduction models have been proposed to explain the non-Fourier conductive heat-transfer behavior in a very short period of time. These include the macro-hyperbolic model[1] and Tzou's dual-phase model.[2] The purpose of the present work is to present a numerical solution to the macrohyperbolic heat-conduction (HHC) model in temperature-dependent materials. Both the analytical[3] and numerical[4–8] methods have been used in solving HHC equation over the years. Glass et al.[4] studied the effects of temperature-dependent thermal conductivity on the thermal wave propagation by using the MacCormack's predictor-corrector scheme. Kar et al.[5] solved a nonlinear HHC equation both analytically and numerically by using the Kirchhoff transformation to linearize the nonlinear terms. However, only one-dimensional problems were considered in their works.[4,5] Present numerical approach employs the Roe–Sweby's total-variation-diminishing (TVD)[9] scheme to solve two-dimensional HHC equations. This scheme was used in a previous study for HHC in composite media.[7] The present work investigates the effects of temperature-dependent properties on the thermal wave propagation in a homogeneous medium.

Mathematical Formulations and Numerical Method

The same form of governing equations of HHC is used in this paper as shown in a Ref. 8, which includes an energy equation and two heat-flux equations:

$$\frac{\partial T}{\partial t}+\frac{1}{\rho C_p}\frac{\partial q_x}{\partial x}+\frac{1}{\rho C_p}\frac{\partial q_y}{\partial y}=\frac{s}{\rho C_p} \tag{1a}$$

$$\frac{\partial q_x}{\partial t}+\frac{k}{\tau}\frac{\partial T}{\partial x}=-\frac{q_x}{\tau} \tag{1b}$$

$$\frac{\partial q_y}{\partial t}+\frac{k}{\tau}\frac{\partial T}{\partial y}=-\frac{q_y}{\tau} \tag{1c}$$

It is assumed that τ remains constant, while k, α, ρ, and C_p change with temperature. Because $\alpha=k/\rho C_p$, the influences of ρ and C_p can be included in the ratio of α/k. With the assumption of $k=k_0(1+\beta T)$ and $\alpha/k=\alpha_0/k_0(1+\gamma T)$, the effect of k on the thermal wave propagation can be observed by changing the value of β, and the combined effects of α, ρ, and C_p on the thermal wave propagation can be obtained by varying the value of γ. Equation (1) is nondimensionalized, and the detailed procedure of nondimensionalization can be seen in a Ref. 8. After nondimensionalization, the equations can be written in a vector form as

$$\frac{\partial \boldsymbol{U}}{\partial t}+\frac{\partial \boldsymbol{E}}{\partial x}+\frac{\partial \boldsymbol{F}}{\partial y}=\boldsymbol{S} \tag{2}$$

where

$$\boldsymbol{U}=[T,q_x,q_y]^T,\qquad \boldsymbol{E}=[(1+\gamma T)q_x,(1+0.5\beta T)T,0]^T$$

$$\boldsymbol{F}=[(1+\gamma T)q_y,0,(1+0.5\beta T)T]^T$$

$$\boldsymbol{S}=[(1+\gamma T)(s/2),-2q_x,-2q_y]^T$$

Equation (2) is transformed from the Cartesian coordinates to the computational coordinates (ξ, η) and is solved by a fractional step method of Roe–Sweby's TVD scheme.[9] This scheme is second-order accurate in the smooth region and first order in the vicinity of discontinuities:

$$\boldsymbol{U}^*_{j,k}=\boldsymbol{U}^n_{j,k}-(\Delta t/\Delta\xi)J_{j,k}\left(\bar{\boldsymbol{E}}^n_{j+\frac{1}{2},k}-\bar{\boldsymbol{E}}^n_{j-\frac{1}{2},k}\right)+\tfrac{1}{2}(\Delta t/\Delta\xi)J_{j,k}\bar{\boldsymbol{S}}^n_{j,k} \tag{3a}$$

$$\boldsymbol{U}^{n+1}_{j,k}=\boldsymbol{U}^*_{j,k}-(\Delta t/\Delta\eta)J_{j,k}\left(\bar{\boldsymbol{F}}^*_{j,k+\frac{1}{2}}-\bar{\boldsymbol{F}}^*_{j,k-\frac{1}{2}}\right)+\tfrac{1}{2}(\Delta t/\Delta\eta)J_{j,k}\bar{\boldsymbol{S}}^*_{j,k} \tag{3b}$$

where J is the Jacobian matrix. A more detailed description on the computational steps is presented elsewhere.[8]

Results and Conclusion

Example 1: Rectangular Cavity with Linear Boundary Conditions

The first example is a rectangular cavity with insulated top and bottom boundaries. A grid system of 400×40 control volumes is used, which gives a grid-independent solution, and Courant–Friedrichs–Lewy is kept at a constant value of 0.5. The dimensionless temperature in the rectangular cavity is initially 1.0 everywhere, and there is no heat generation inside the rectangular cavity. For time $t>0$, a periodic on–off heat flux is supplied to the left boundary ($\xi=0$), and the dimensionless temperature at the right boundary ($\xi=1$) is kept at 1.0. The periodic on–off heat flux is prescribed by[6]

$$f(t)=\begin{cases}1.0 & (i-1)P<t<[(i-1)+\kappa]P\\ 0 & [(i-1)+\kappa]P<t<iP\end{cases}\qquad i=1,2,3,\ldots \tag{4}$$

where i represents the number of periods and P is the period. Here we choose $\kappa=0.5$ and $P=0.1$.

The effect of k on the thermal wave propagation can be observed by changing the value of β, and the combined effects of α, ρ, and C_p on the thermal wave propagation can be obtained by varying the value of γ. The influences of β and γ on the thermal wave propagation are plotted in Figs. 1 and 2, respectively at $t=0.8$.

Received 17 July 2003; revision received 13 November 2003; accepted for publication 14 November 2003.

*Graduate Student, Department of Mechanical Engineering; currently Ph.D. Candidate, Department of Computer Science, The University of Kentucky.

†Professor, Department of Mechanical Engineering. Member AIAA.